An optimal process of femtosecond laser cutting of NiTi shape memory alloy for fabrication of miniature devices

Li, Chengde; Nikumb, Suwas; Wong, Franklin

Publisher's version / Version de l'éditeur:
https://doi.org/10.1016/j.optlaseng.2005.08.003
Optics and Lasers in Engineering, 44, 10, pp. 1078-1087, 2006-10

An optimal process of femtosecond laser cutting of NiTi shape memory alloy for fabrication of miniature devices

Chengde Li [1], Suwas Nikumb [2], and Franklin Wong [3]

(1) Department of Applied Physics, School of Science, Beijing Institute of Technology, Beijing 100081, China

(2) Integrated Manufacturing Technologies Institute, National Research Council of Canada, London, Ontario, N6G 4X8, Canada (Fax: 1-(519)430-7064 Email: Suwas.Nikumb@nrc.ca)

(3) Defense Research & Development Canada, Valcartier, Val Belair, Quebec, G3J 1X5, Canada

Abstract:

The mechanical properties of NiTi shape memory alloy (SMA) components are sensitive to thermal influence during laser machining. To make the femtosecond laser cutting of NiTi material meet the strict fabrication requirements for miniature SMA devices with high precision, complex patterns and minimal heat affected zone (HAZ) along with high throughput, we report an optimal process of sideways-movement path planning in this article. Femtosecond laser processing of NiTi SMA using the fundamental wavelength of 775 nm from a Ti:sapphire laser along with its second and third harmonic irradiations were systematically investigated. We observed that the main impact of ultrashort laser pulse induced air breakdown on materials processing was beam widening. The laser beam at fundamental wavelength suffered less widening than its harmonic wavelengths. Femtosecond laser machining of metals is still basically a thermal mechanism. High ablation rates at higher laser fluences causes significant recast formation, while lower fluences resulted in better cutting quality at the expense of efficiency. The optimal process involving the method of sideways-movement path planning enables recast-free high precision features at higher laser fluences with better throughput.

PACS: 42.65.Re; 42.62.Cf; 81.05.Bx; 81.40.

1. Introduction

Micro-electromechanical systems (MEMS) based miniature devices have received significant attention in several branches of science and technology for a variety of applications. Amongst various micro-actuation mechanisms that include piezoelectric, electrostatic, magnetic, bimetal and shape memory alloy materials, NiTi shape memory alloys (SMA) are important not only because they enable large displacements and high actuation force [1], but also because they are inherently biocompatible [2]. Since the NiTi SMA components are thermally operated between the transformation temperatures of martensite and austenite, the mechanical properties of the microfabricated devices are sensitive to thermal influences. Therefore, heat affect zones and residual stresses have to be minimized during the laser fabrication process so as to keep their functional properties unaffected. In recent literature, laser drilling of small holes on thin NiTi wires [3], patterning on NiTi thin film on silicon substrates [4, 5] and cutting of rolled NiTi sheets [6] have been studied using Q-switched solid state nanosecond laser, excimer UV lasers and IR femtosecond lasers. However, the process control necessary to obtain the required precision during processing of these thermally sensitive materials and its effect on the mechanical behavior is still not fully understood.

In the past decade, the interaction of ultrashort laser pulses with a variety of materials has been studied intensively. The advantages of ultrashort pulse lasers over more conventional nanosecond pulsed lasers in material processing have been recognized. Since the laser processing of metals using ultra-short pulse duration is still basically a

thermal process, the amount of recast formation during drilling and cutting processes significantly reduces as the pulse duration decreases, but is never eliminated fully[7]. The heat-affected zones usually extend in microns range [8, 9]. The deformation of beam profile caused by ultrashort laser pulse induced breakdown of air has also been reported [10]. By reducing the laser fluence to a value slightly above the ablation threshold at the expense of throughput and costs has resulted in high precision machining without burr formation.

In this article, a systematic investigation of femtosecond laser processing of NiTi SMA using a fundamental wavelength of 775 nm from Ti:Saphire laser and its second and third harmonic irradiations is reported. A thermal-influence-free optimal process was developed to fabricate complex miniature SMA components. In addition, we demonstrate a sideways-movement path planning technique to enable higher laser fluences for improved throughput processing and achieving recast-free, high precision features.

2. Experimental

A Clark MXR CPA-2010 femtosecond laser system was used in these experiments. The laser delivered 150 fs pulses with an average power of 1W at the fundamental wavelength of 775 nm. An integrated harmonic generator provided an average power of 250 mW at the second harmonic wavelength of 387 nm and 80 mW at the third harmonic wavelength of 258 nm. The laser system was operated at a pulse repetition rate of 1 kHz. The beam of 775 nm fundamental wavelength was focused using a microscope objective (CVI Laser Co.) with focal length of 21mm and a NA of 0.23. The second harmonic and third

harmonic laser beams were focused with objectives suitable to the respective wavelengths. Laser beam intensity reaching the sample surface was controlled with neutral density filters. Beam expanders were used for collimating purposes. The plasma column at the geometry region was imaged using a MEIJI EMZ-TR stereo microscope with color CCD side camera. Laser intensity distribution behind the focal region was measured using a beam diagnostic system (Big Sky Laser Technologies, Inc.).

The SMA samples used in our experiment were 220 μm thick, cold rolled sheets (Special Metals Co.) with a chemical composition of 55.88Ni-44.11Ti . The samples were mounted on a CAD/CAM driven motion stage with a specially developed pumping holder/fixture to avoid surface distortions, striations and unevenness. For the measurements of the laser material removal rate, the samples were machined using a multiple-pass laser scanning method. The average removal rate was obtained as a ratio of material thickness to the number of laser scans required to cut the samples through fully. Then ablation depth per pulse was calculated. A Hitachi S3500N SEM was used for characterization of the processing quality.

3. Results and Discussion

In general, to obtain high throughput production processing, higher laser fluences are required. For machining using ultrashort laser pulses with high average power, the influence of laser induced air breakdown at the focal region must be taken into account. In these experiments, the femtosecond laser induced air breakdown plasma in the focal region was observed at pulse energy > 40 μJ at the fundamental wavelength of 775 nm.

For the third harmonic wavelength at 258 nm, very strong plasma was observed at the pulse energy as low as 10 μJ. Fig. 1 illustrates the plasma generation and a part of the 3-dimensional beam profile behind the laser focus. It is obvious that a large amount of beam energy was scattered into the surrounding ring structure [11]. However, it is important to note that all of the measurements on the beam profiles were performed at a position far behind the laser focal region. Indeed, if mask image projection technique were to be used for patterning materials, this distortion to wavefront would have harmed the process greatly. In the case of machining with a focused laser beam, the surface of workpiece is placed in focal region as shown in Fig. 1 (b). The intensity distribution in the focal region could be non-ring-structure.

For a Gaussian beam the diameter D of the ablated zone is related to the incident laser fluence F, threshold ablation fluence F_{th} and the beam focus diameter D_0 by [7]

$$D = D_0 \sqrt{\frac{1}{2} \ln \frac{F}{F_{th}}} \qquad (1)$$

This relationship predicts that machining features much smaller than the laser's focal spot size, even down to sub-optical-limit, are possible using femtosecond lasers [12]. However, Eq. (1) is not applicable when laser induced air breakdown is present. As shown in Fig. 2, the cutting width is wavelength dependent. In the case of the third harmonic wavelength, as the fluence of laser irradiation increases from 3 J/cm^2 to 25 J/cm^2, the cutting width increased to more than 40%. Widening to the same percentage, for the second harmonic, a fluence of 40J/cm^2 was required while nearly 70J/cm^2 was needed for the fundamental wavelength. This is due to the fact that UV photons have higher energy in comparison to

the infrared photons for ionizing the air atoms and producing a plasma column with larger dimensions. This also means that for higher beam fluences cutting with the fundamental wavelength of the laser achieves narrower channels compared to the second and the third harmonic radiation.

Fig. 3 shows the ablation depth per scan at different scan speeds for the three wavelengths. It is noteworthy that the ablation depth is less than 5 μm/ scan at a scan speed of 60 mm/min or higher up to a laser fluence of 45 J/cm$^{2.}$ These values indicate that a high degree of the ablation depth control is possible. Fig. 4 shows shallow tracks cut with a single laser scan at speeds of 10 mm/min, 30mm/min, 60 mm/min, 100 mm/min and 300mm/min, respectively. It is clear that the faster the scan rate, the smoother the track and the less heat dissipation there is to the surrounding material.

Figure 5 shows the calculated average volume ablation rate in μm^3 per pulse using the data from Fig.3. It reveals that volume ablation rate, i. e. cutting efficiency is almost the same for different scan speeds for a given laser fluence. This suggests that, high speed scanning yields better results compared to scanning at slow speeds and that scanning speeds must be considered during optimization of the cutting process.

In nanosecond and longer pulsed laser machining of metals, it is well known that the energy shielding effect of the plasma plume formed by ejecting materials from the ablation crater greatly lowers the efficiency of laser energy coupling to the work piece. Furthermore, machining quality suffers from this plasma plume that causes prolonged

heating and melting effects [13]. These effects can be reduced using UV wavelengths from nanosecond laser ablation of materials [14]. However, Fig. 6 (a) makes it clear that in the case of femtosecond laser ablation, the volume ablation rate in μm^3 per pulse increases with the laser fluence without saturation. Besides, there is no significant difference regarding ablation efficiency between the three wavelengths. This fact indicates that the energy shielding effect of the ablated plume is absent in the case of femtosecond laser machining. It also reveals that the air breakdown plasma in the focal region is not an energy-consuming phenomenon.

The calculated dependence of ablation depth per pulse on the laser fluence shown in Fig. 6 (b) indicates that the ablation depth is as small as tens of nanometers for laser fluences lower than 15 J/cm^2, meaning that highly precise, recast free cutting surfaces are possible. The disadvantage of this low fluence cutting method is low throughput for production applications. The ablation depth per pulse at harmonic wavelengths is slightly lower than that at the fundamental wavelength because of the air plasma widening effect discussed above. Since the laser fluence of the fundamental wavelength is higher than 25 J/cm^2, the average ablation rate is as high as 0.1 μm/pulse. However, high fluence cutting causes prominent, visible recast deposites around the edges of the ablation site. Fig. 7 shows a channel cut with laser spot size of 36 μm at a fluence of 40 J/cm^2 and at scanning speed of 60 mm/min. Rough cut edge morphology and a little recast layer on the edges of the cut is evident.

In order to make the process of femtosecond laser cutting NiTi materials more viable and able to meet the precision requirements for machining miniature SMA devices with a high throughput, we explored a novel method in tool path planning. The idea of sideways motion path is schematically shown in Fig. 8. Initially, high fluence fundamental femtosecond laser beam scans at high speed along the designed tool path. Then a second scan is deployed by changing the location of the laser spot sideways about 1 μm towards one edge with respect to its nominal path position. This is followed by a third scan once again by changing the location of the laser focal spot sideways about 1 μm with respect to the nominal path position towards the opposite edge and completes one routine. Figure 9 shows a slot with a width of 40 μm that was cut at a laser fluence of 40 J/cm^2 using the new path planning method. The spot size and the scan speed were unchanged from that used in Fig. 7. Two 1 μm sideways movements were applied to each side in the routines for this example. It can be seen that the cutting quality was improved greatly, at the cost of an additional ~10% of time required for the cutting process.

Sideways-movement path planning takes advantages of both high laser fluence for increasing the throughput and low laser fluence for improving feature precision. We attribute the smooth cutting edge to threshold fluence trimming and air plasma milling. Because the transverse intensity distribution in a femtosecond laser beam decreases sharply from center outwards, in the step 2 and 3 of the above process routine, the outer rim of the laser beam trims the material gently at a fluence just above the ablation threshold. Secondly, the femtosecond laser induced air plasma column mills the work

piece by removing the recast deposited on the edges of the cut during the step 1. The heat-affected regions at the edges can thus be polished away due to these two effects.

Fig. 10 (a) displays a section of a complex pattern of NiTi SMA material, fabricated with the above optimal femtosecond laser processing method. Clean polished edges, curves and cuts are evident. Fig. 10 (b) shows an enlarged SEM image (500 ×) of a portion of the component. No recast layer was observed.

4. Conclusion

In conclusion, the impact of ultrashort pulses induced air breakdown on femtosecond laser materials processing is beam widening. The laser beam at a fundamental wavelength of 775 nm suffers much less widening than at its harmonic wavelengths of 387 nm and 258 nm. Femtosecond laser machining of metals is still basically a thermal mechanism. High ablation rate cutting with high laser fluence causes significant recast, while lower beam fluences result in high cutting quality at the cost of efficiency. The novel optimal process of sideways-movement path planning enables the use of high laser fluences for better process throughput and high quality, recast-free, precision features. This optimized process is particularly useful for the fabrication of precision miniature devices based on NiTi shape memory alloys and other similar materials.

Acknowledgements

The authors would like to acknowledge M. Islam, Director, Production Technology Research, for his support, and Hugo Reshef, Craig Dinkel and Mike Meinert for their

technical assistance. This work was partially funded through the Defence Research & Development Canada Technology Investment Fund under the project entitled 'Supersonic Missile Flight Control by Manipulation of the Flow Structure using Microactuated Surfaces'.

References

1. P. Krulevitch, A. P. Lee, P. B. Ramsey, J. C. Trevino, J. Hamilton and M. A. Northrup, J. Microelectromech. Syst., **5**, 270 (1996)

2. F. Villermaus, M. Tabrizian, L. H. Yahia, M. Meunier, D. L. Piron, Appl. Surf. Sci. **109/110**, 62 (1997)

3. H. Haferkamp, S. Paschko, F. von Alensleben, M. Goede, Actuator 2000, 7th Inter. Conf. On New Actuator, **19** (2000)

4. W. M. Huang, Q. He, M. H. Hong, Q. Xie, Y. Q. Fu, and H. J. Du, SPIE **4915**, 234 (2002)

5. A. J. Dowling, M. K. Ghantasala, J. P. Hayes, E. C. Harvey, and E. D. Doyle, Smart. Mater. Struct. **11**, 715 (2002)

6. H. Y. Zheng, A. R. Zareena, H. Huang and G. C. Lim, Mater. Sci. Forum, **437/438**, 277 (2003)

7. F. Dausinger, RIKEN Review, 50, **77** (2003)

8. A. Luft, U. Franz, A. Emsermann, J. Kaspar, Appl. Phys. **A 63**, 93 (1996)

9. R. Le Harzic, N. Huot, E. Audouard, C. Jonin, and P. Laporte, Appl. Phys. Lett. **80**, 3886 (2002)

10. J. Sun and J. P. Longtin, J. Appl. Phys. **89**, 8219 (2001)

11. S. L. Chin, N. Akozbek, A. Proulx, S. Petit, C. M. Bowden, Opt. Commun. **188**, 181 (2001)

12. P. P. Pronko, S. K. Dutta, J. Squier, J. V. Rudd, D. Du, G. Mourou, Opt. Commun. **114**, 106 (1995)

13. J.J. Chang, and B. E. Warner, Appl. Phys. Lett. **69**, 473 (1996)

14. S. V. Govorkov, E. V. Slobodchikov, A. O. Wiessner, D. Basting, SPIE, **4065**, 790 (2000)

Captions

Fig. 1 (a) A portion of a 3-D ring structure of fs laser beam profile behind focus. The insertion on the upper right is the air plasma column causing the beam deformation (b) Schematic of femtosecond laser focal region intersecting with workpiece. The intensity distribution in the focal region could be non-ring-structure.

Fig. 2 The relation of cutting width with energy density is wavelength dependent.

Fig. 3 Ablation depth per scan at different scan speeds for three wavelengths: 775 nm, 387 nm and 258 nm.

Fig. 4 Shallow tracks cut with single laser scan at speed 10 mm/min, 30mm/min, 60 mm/min, 100 mm/min and 300mm/min from above to below, respectively. The faster the scan, the smoother is the track and less heat load is in the material.

Fig. 5 Average volume ablation rate for different feed rate at same fluence.

Fig. 6 (a) The dependence of volume ablation rate in μm^3 per pulse on laser fluence (b) The dependence of ablation depth in μm per pulse on laser fluence.

Fig. 7 Prominent recast is found around the channel cut with femtosecond laser fluence as high as 40 J/cm^2.

Fig. 8 Sideways-movement path planning to get rid of recast and minimize HAZ for high throughput femtosecond laser cutting at high fluence

Fig. 9 A slot of 40 μm in width cut at laser fluence of 40 J/cm^2 with sideways-movement path planning.

Fig. 10 (a) A NiTi SMA self-expanding medical micro-device fabricated with the optimal femtosecond laser process. (b) An enlarged SEM image of a portion of the component.

Figures

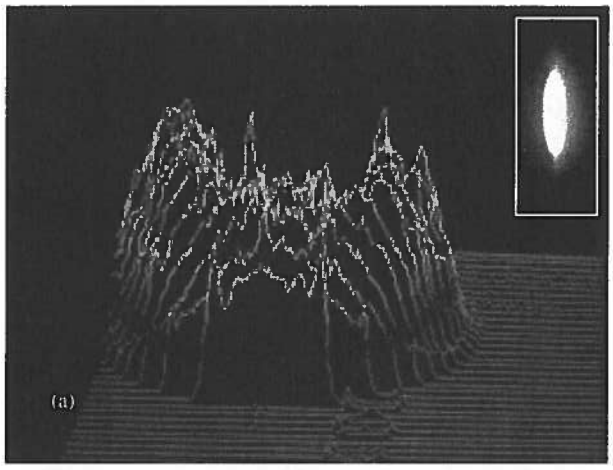

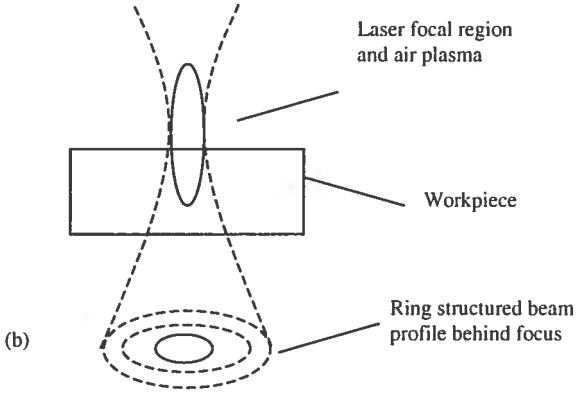

Fig. 1

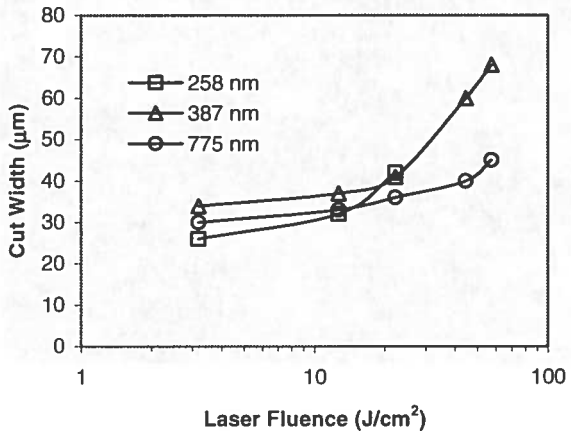
80
70
60
50
40
30
20
10
0
Cut Width (µm)
258 nm
387 nm
775 nm
1
10
100
Laser Fluence (J/cm²)

Fig.2

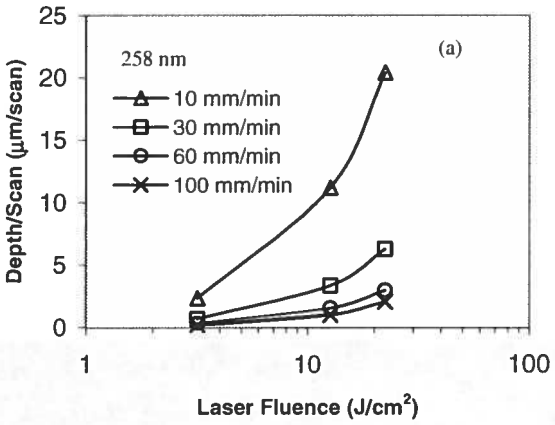
258 nm
(a)
10 mm/min
30 mm/min
60 mm/min
100 mm/min
Depth/Scan (µm/scan)
Laser Fluence (J/cm²)

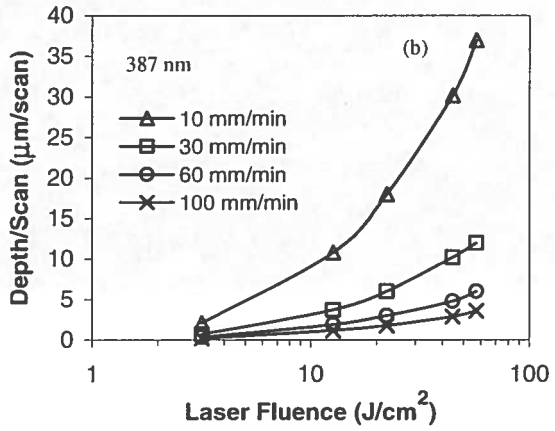
387 nm
(b)
10 mm/min
30 mm/min
60 mm/min
100 mm/min
Depth/Scan (µm/scan)
Laser Fluence (J/cm²)

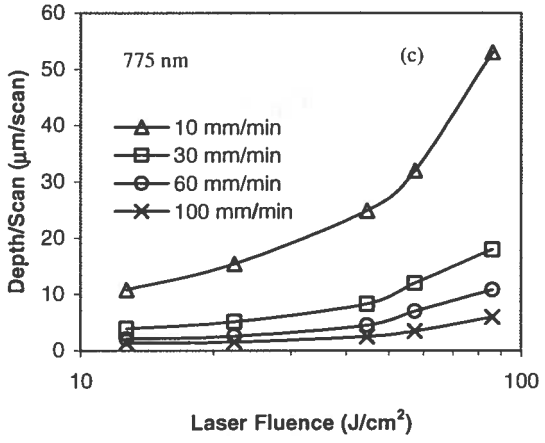
775 nm
(c)
10 mm/min
30 mm/min
60 mm/min
100 mm/min
Depth/Scan (µm/scan)
Laser Fluence (J/cm²)

Fig. 3

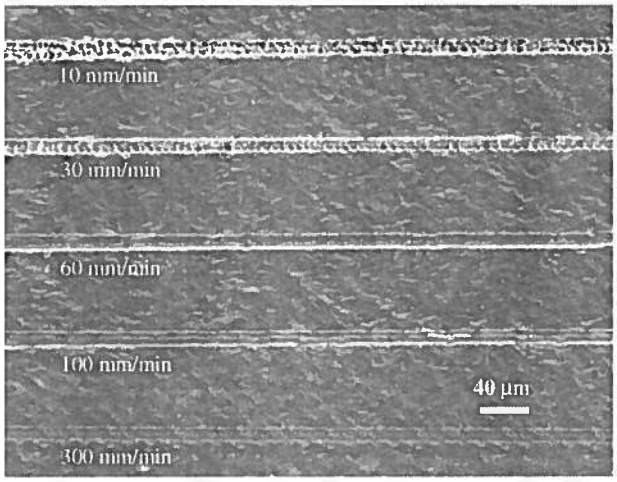

Fig. 4

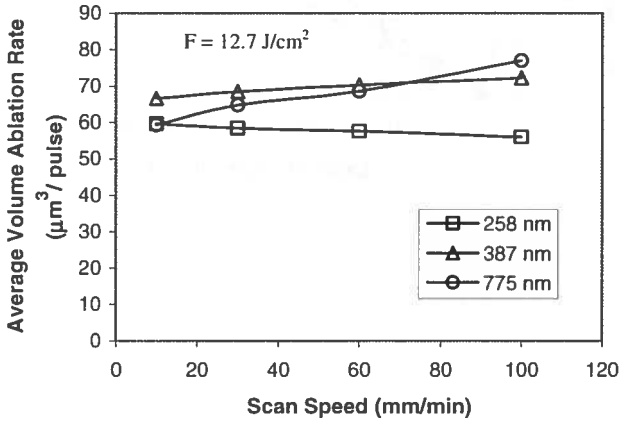
F = 12.7 J/cm²
Average Volume Ablation Rate (μm³/ pulse)
Scan Speed (mm/min)
258 nm
387 nm
775 nm
0
10
20
30
40
50
60
70
80
90
0
20
40
60
80
100
120

Fig. 5

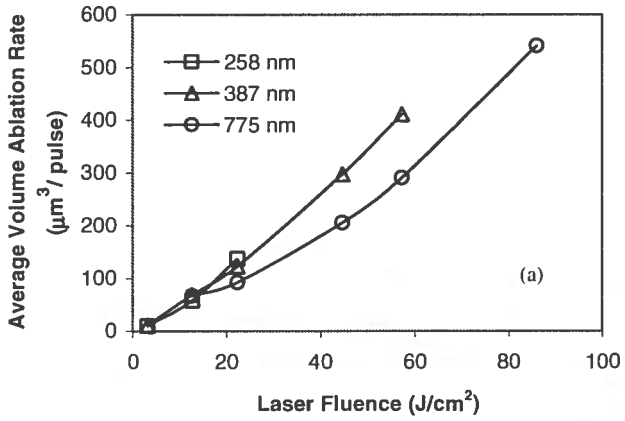
Average Volume Ablation Rate (μm³/pulse)
600
500
400
300
200
100
0
258 nm
387 nm
775 nm
(a)
0
20
40
60
80
100
Laser Fluence (J/cm²)

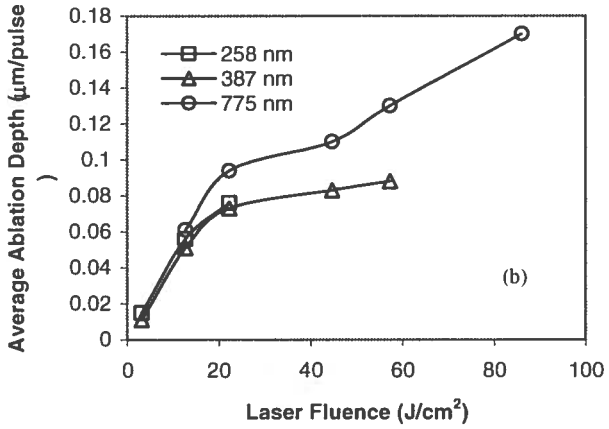
Average Ablation Depth (μm/pulse)
0.18
0.16
0.14
0.12
0.1
0.08
0.06
0.04
0.02
0
258 nm
387 nm
775 nm
(b)
0
20
40
60
80
100
Laser Fluence (J/cm²)

Fig. 6

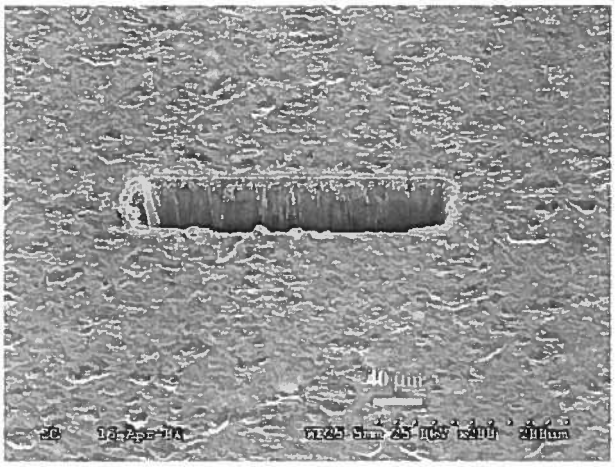

Fig. 7

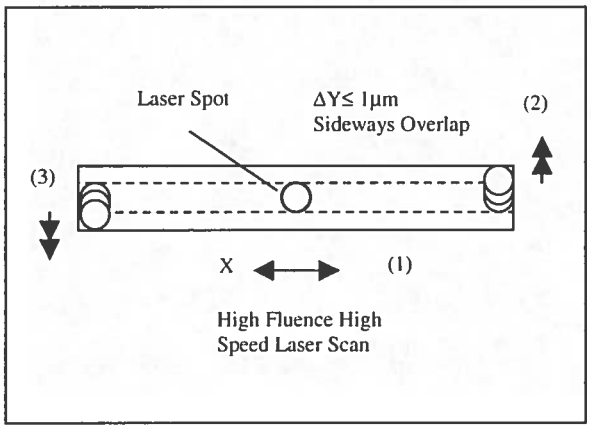
Laser Spot
ΔY≤ 1μm
Sideways Overlap
(2)
(3)
X
(1)
High Fluence High
Speed Laser Scan

Fig. 8

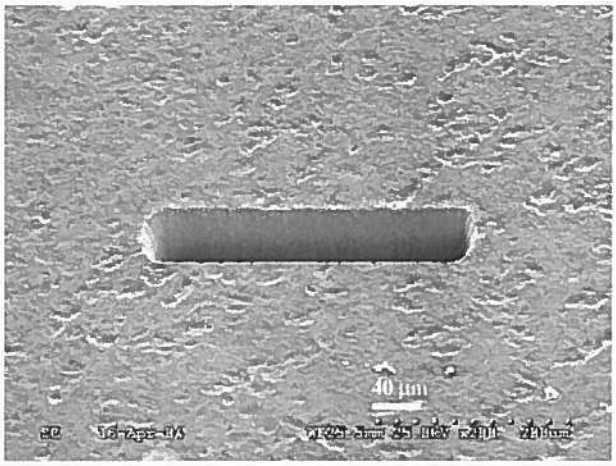

Fig. 9

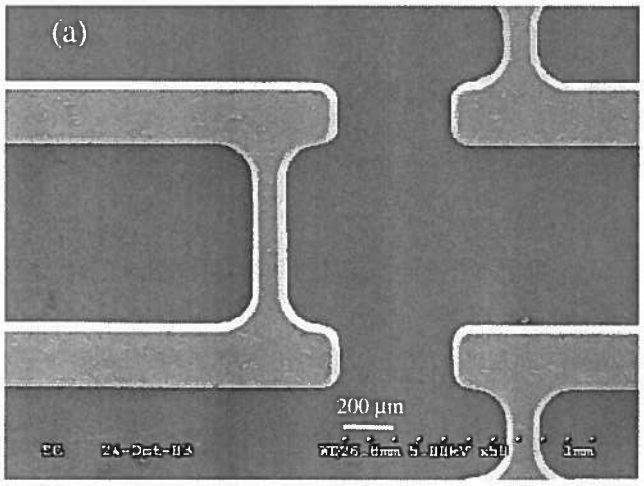

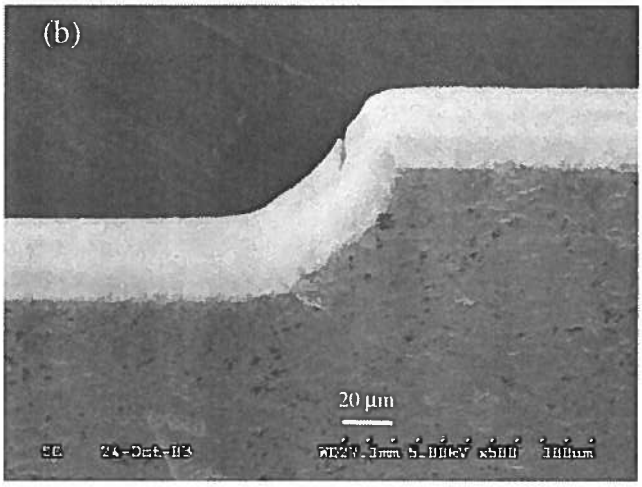

Fig.10